World Scientific
www.worldscientific.com

JSCE
JAPAN SOCIETY OF CIVIL ENGINEERS
COASTAL ENGINEERING COMMITTEE

Coastal Engineering Journal, Vol. 48, No. 1 (2006) 59–79

NUMERICAL SIMULATION OF LONG-PERIOD WAVES AND SHIP MOTIONS IN TOMAKOMAI PORT, JAPAN

WIM VAN DER MOLEN
Faculty of Civil Engineering,
Delft University of Technology,
Delft, The Netherlands
W.vanderMolen@citg.tudelft.nl

PATRICIO MONÁRDEZ
UNESCO-IHE Institute for Water Education,
Delft, The Netherlands,
presently at Baird and Associates, Santiago, Chile
pmonardez@baird.com

AP VAN DONGEREN
WL|Delft Hydraulics and Delft University of Technology,
Delft, The Netherlands
Ap.vanDongeren@wldelft.nl

Received 18 March 2005
Revised 16 December 2005

Long waves can penetrate easily into ocean facing ports or even be amplified if the wave frequency is close to one of the natural frequencies of the harbor. Moreover, the moored ship can have its natural frequency close a natural frequency of the basin, so that large ship motions can occur at relatively low offshore wave heights. Correct prediction (using e.g. numerical models) of long wave penetration and amplification is important in the design of new ports or port expansions. In this work, numerical simulations are presented using a wave model that accounts for the generation and propagation of bound and free long waves. The forces on the moored ship are calculated using the time-series of wave elevations and fluid motions at the location of the ship applying a strip theory approach. The ship motions are simulated using the calculated exciting wave forces, considering the non-linear characteristics of fenders and mooring lines. The numerical results are compared with prototype measurements carried out during a typhoon event in the port of Tomakomai in Japan and show good agreement.

Keywords: Long-period waves; moored ships; strip theory; numerical methods.

1. Introduction

Long waves which affect harbor operations typically have periods between 30 and 300 seconds. Collectively known as infragravity waves, these waves include free oceanic waves and so-called "bound" or "locked" waves, which are forced by grouped sea-swell waves. These bound waves propagate at the group velocity, are 180° out of phase with the short-wave envelope and have amplitudes proportional to the square of the sea-swell wave heights. The development of the theory describing these waves started with the first field observations made by Munk [1949] and Tucker [1950] who reported that the temporal variation of incident short-wave heights in groups of waves is responsible for the presence of infragravity waves in the near-shore. Munk introduced the term "surf beat" to indicate the long waves that propagate back out to sea when groups of short waves break on a beach. Biésel [1952] and later Longuet-Higgins and Stewart [1962, 1964] found that bound waves are forced by short wave groups. Mathematically, the forced wave number and frequency are characterized by the differences of wave numbers $k_n - k_m$ and wave frequencies $f_n - f_m$ from all possible pairs m, n of short-wave components that can be formed in one spectrum. Similarly, bound waves travelling over an uneven bathymetry can be partially released as free waves [Dingemans *et al.*, 1991]. In case of small incidence angles, the free infragravity wave reflects and is able to escape (or leak) to deeper water but for larger angles of incidence the free infragravity wave may become refractively-trapped as an edge wave.

Incoming low-frequency bound and released (free) waves can drive harbor seiches at the group frequency without breaking; this has been shown theoretically [Bowers, 1977; Wu and Liu, 1990] and in laboratory experiments [Bowers, 1977]. When energetic, the large oscillatory horizontal displacement caused by these low frequency oscillations can seriously interfere with harbor operations, causing costly delays and extreme motion and damage to ships, as was reported by Hiraishi *et al.* [1997].

The aim of the present study is to validate a train of numerical methods of calculating the long wave motion, and the resulting forces and motions of the ship due to these waves. Previously developed methods that include such a train of numerical methods were either fully linear [e.g. Ohyama and Tsuchida, 1997] or nonlinear with respect to the incident waves [Bingham, 2000]. The present method is linear with respect to the incident short waves, but nonlinear with respect to the associated bound waves and the free long waves. For the calculation of the propagation of both forced and free long waves, the depth-averaged non-linear shallow water flow model Delft3D-Surfbeat [Reniers *et al.*, 2000, 2004] is used, which incorporates a 2D energy propagation and dissipation model for the short waves which is used to force the long waves. The model considers the directionally-spread wave energy, associated with wave groups, propagating shoreward with the wave group celerity along precalculated mean wave directions. The presence of the moored ship is not taken into account in this wave model directly. The forces on the ship are computed using

a strip theory approach on the calculated long wave elevations and particle velocities [Van der Molen *et al.*, 2003]. The external forces and moments in the model are composed by forces due to incoming waves, hydrodynamic reaction forces due to ship motions, hydrostatic restoring forces, viscous damping forces, mooring line forces and fender forces. Due to the nature of the mooring arrangement and in particular of the fender characteristics, moored vessels are known to exhibit a distinct non-linear behavior. This implies that the mathematical description has to be based on a time domain formulation, relating instantaneous values of forces and motions. For these reasons, the motions of the ship are calculated using the time-domain ship motion simulation model BAS [Mynett *et al.*, 1985], which takes into account the hydrodynamic properties of the ship and the non-linear characteristics of fenders and mooring lines.

Van Giffen *et al.* [2003] compared calculations using the same shallow water hydrodynamic model with measurements carried out in Saldanha Bay, South Africa, and found good agreement for the lowest frequencies while the waves at higher infragravity frequencies were overpredicted. A possible explanation for the overprediction is the lack of damping of higher-frequency long waves reflecting off a beach or a breakwater. They did not consider wave forces and ship motions. Van der Molen *et al.* [2003] used the same approach for the calculation of infragravity waves as well as wave forces on the ship and compared with model tests taken at the Vinje directional wave basin at WL|Delft Hydraulics, The Netherlands. They found good correspondence for the waves and forces at the frequencies of the lowest two resonant modes of the harbor basin. The higher modes were underpredicted, probably because of spurious oscillations in the laboratory basin.

In this paper, which is based on the work by Monárdez [2004], the model train is applied to a real situation and compared with measurements of waves and surge motions of a coal carrier during a typhoon event in Tomakomai Port, Japan [Hiraishi *et al.*, 1997]. The paper contains in Sec. 2 the governing equations of the nonlinear shallow water model and the model for low-frequency wave forces on a ship. Section 3 describes the port layout, ship description, mooring conditions and field measurements. Section 4 contains the simulations of infragravity waves. Section 5 refers to the simulation of long-wave exiting forces and ship motions. Section 6 proposes mitigation measures and Sec. 7 contains the conclusions and recommendations from the research.

2. Numerical Model

2.1. *Governing equations of the nonlinear shallow water model*

For the calculation of infragravity wave penetration in the harbor, the "Surfbeat" module in Delft3D as developed by WL|Delft Hydraulics is used. The module solves the nonlinear shallow water equations of mass and momentum with radiation stress

forcing provided by the concurrently solved energy equations of the organized short wave motion and the roller on the time scale of the wave groups [Reniers *et al.*, 2004]. The model is capable of simulating both bound (radiation-stress forced) and free long waves.

The governing equations of mass and momentum can be written as

$$\frac{\partial \eta}{\partial t} + \frac{\partial (hu)}{\partial x} + \frac{\partial (hv)}{\partial y} = 0 \tag{1}$$

where η is the surface elevation of the long wave motion, h is the total depth, u and v are the x and y components of the long-wave particle velocities, and

$$\begin{aligned} \frac{\partial u}{\partial t} + u\frac{\partial u}{\partial x} + v\frac{\partial u}{\partial y} = &-F_x - g\frac{\partial \eta}{\partial x} + \frac{1}{h}\frac{\partial}{\partial x}\left(2\nu_t h\frac{\partial u}{\partial x}\right) \\ &+ \frac{1}{h}\frac{\partial}{\partial y}\left(\nu_t h\frac{\partial u}{\partial y}\right) + \frac{1}{h}\frac{\partial}{\partial y}\left(\nu_t h\frac{\partial v}{\partial x}\right) - \tau_x \end{aligned} \tag{2}$$

$$\begin{aligned} \frac{\partial v}{\partial t} + u\frac{\partial v}{\partial x} + v\frac{\partial v}{\partial y} = &-F_y - g\frac{\partial \eta}{\partial y} + \frac{1}{h}\frac{\partial}{\partial x}\left(\nu_t h\frac{\partial v}{\partial x}\right) \\ &+ \frac{1}{h}\frac{\partial}{\partial x}\left(\nu_t h\frac{\partial u}{\partial y}\right) + \frac{1}{h}\frac{\partial}{\partial y}\left(2\nu_t h\frac{\partial v}{\partial y}\right) - \tau_y \end{aligned} \tag{3}$$

Here ν_t is the eddy viscosity, which is 0.1 m^2/s outside the breaker zone and increases in value due to breaking. The area of application for the present study is outside the breaker zone, however. τ_x and τ_y are the bottom friction terms expressed in terms of vertical velocity gradients according to Rodi [1980]. The forcing is given by the radiation stress gradients

$$F_x = \frac{1}{\rho h}\left(\frac{\partial S_{xx}}{\partial x} + \frac{\partial S_{yx}}{\partial y}\right) \tag{4}$$

$$F_y = \frac{1}{\rho h}\left(\frac{\partial S_{yy}}{\partial y} + \frac{\partial S_{xy}}{\partial x}\right) \tag{5}$$

The radiation stresses are expressed as composed of a contribution of the organized wave energy E_w and of the roller energy E_r

$$S_{xx} = \left(\frac{c_g}{c}(1+\cos^2\theta) - \frac{1}{2}\right)E_w + 2E_r\cos^2\theta \tag{6}$$

$$S_{xy} = \left(\frac{c_g}{c}\cos\theta\sin\theta\right)E_w + 2E_r\cos\theta\sin\theta \tag{7}$$

$$S_{yy} = \left(\frac{c_g}{c}(1+\sin^2\theta) - \frac{1}{2}\right)E_w + 2E_r\sin^2\theta \tag{8}$$

where θ is the angle of incidence, c_g is the group speed and c is the linear wave celerity.

The energy in the organized short-wave motion E_w is calculated from the wave energy balance, which is capable of computing directionally-spread wave energy associated with wave groups:

$$\frac{\partial E_w}{\partial t} + \frac{\partial E_w c_g \cos\theta}{\partial x} + \frac{\partial E_w c_g \sin\theta}{\partial y} = -D_w \tag{9}$$

where D_w is the dissipation of the total organized wave motion. The energy in the roller is calculated from the roller energy balance:

$$\frac{\partial E_r}{\partial t} + \frac{\partial 2E_r c \cos\theta}{\partial x} + \frac{\partial 2E_r c \sin\theta}{\partial y} = -D_r + D_w \tag{10}$$

in which the only unknown is the mean angle of incidence θ which is obtained from a wave refraction analysis using the spectral wave model SWAN [Booij *et al.*, 1999]. D_r is the dissipation in the roller only

$$D_r = E_r c^{-1} g \sin\beta \tag{11}$$

with β the roller angle ($\beta \approx 0.1$ rad). The boundary conditions which drive the model are the time variations on the wave group scale of the short-wave energy E_w, the associated bound long waves and free long waves in the infragravity frequency band.

In the pre-processing, the short-wave energy variations on the group-scale are obtained by first calculating the time variation of the surface elevation on the wave scale using amplitude information from a measured sea-swell spectrum above a certain split frequency which separates long and short-wave components, and a random phase model. Then we take the envelope of these motions by Hilbert Transform and apply a low pass filter to obtain variations on the wave group scale. From the short-wave energy variations the associated bound (or set-down) wave can be found. Details of this procedure can be found in Van Dongeren *et al.* [2003]. In addition, free long waves (the components below the split frequency in a measured spectrum) can be specified on the boundary. In the infragravity frequency band, motions therefore consist of bound and free components.

2.2. *Wave force formulations*

For the calculation of ship motions the time-domain simulation model BAS [Mynett *et al.*, 1985] is used. It solves the equation of motion of the ship, which is given by

$$(\mathbf{M}+\mathbf{A})\ddot{\vec{X}}(t) + \mathbf{B}_v \dot{\vec{X}}(t)|\dot{\vec{X}}(t)| + \mathbf{C}\vec{X}(t) + \int_0^\infty \mathbf{K}(\tau)\dot{\vec{X}}(t-\tau)d\tau = \vec{F}(t) \tag{12}$$

where $\mathbf{M}$ is the inertia matrix, $\mathbf{A}$ is the matrix containing the added mass coefficients, $\mathbf{B}_v$ contains the low-frequency viscous damping coefficients, $\mathbf{C}$ the hydrostatic

spring coefficients, **K** the retardation functions containing the effect that the body oscillation is damped due to waves radiating away from the body, $\vec{X}$ represents the ship motion in six degrees of freedom and $\vec{F}$ the exciting forces due to waves, current and wind and the forces in fenders and mooring lines. The hydrodynamic coefficients A_{kj}, C_{kj} and $K_{kj}(t)$ are calculated using the frequency-domain panel model DELFRAC [Pinkster, 1995], taking into account the influence of a quay wall. The exciting wave force is the force acting on the restrained ship in waves. For the calculation of wave forces on the ship, a strip theory approach is utilized in the model "*lf-strip*". Within strip theory the ship is divided into a typical number of 20 cross-sectional strips. The force is calculated for each cross-section separately, F'_k, and then integrated over the ship length to provide the total wave force

$$F_k = \int_L F'_k dx \quad k = 1, 2, \ldots, 6 \tag{13}$$

The forcing waves we consider are long waves, so that the Froude-Krylov force due to the incident undisturbed wave is simply equal to the integration of hydrostatic forces over the submerged hull surface. The force due to the disturbance of the incident wave by the presence of the ship is calculated using the relative motion principle, supported by the Haskind relations [Haskind, 1957]. This principle states that the force on a fixed body due to an oscillating fluid is equal to the force due to an oscillating body in still water. Because the infragravity waves are much longer than the dimensions of the cross-section, the wave slope and the horizontal particle velocities and accelerations are assumed to be constant over each cross-section. This reduces the Froude-Krylov forces on the cross-section to very simple formulations for surge, sway, heave and roll:

$$F'_{1,FK}(t) = -\rho g \frac{\partial \eta}{\partial x}(t) \cdot A_x \tag{14}$$

$$F'_{2,FK}(t) = -\rho g \frac{\partial \eta}{\partial y}(t) \cdot A_x \tag{15}$$

$$F'_{3,FK}(t) = \rho g \eta(t) \cdot b_s \tag{16}$$

$$F'_{4,FK}(t) = \rho g \frac{\partial \eta}{\partial y}(t) \cdot \left(\frac{b_s^3}{12} - \overline{bG} \cdot A_x \right) \tag{17}$$

where A_x is the cross-sectional area, b_s is the sectional breadth and $\overline{bG}$ is the vertical distance between the cross-sectional center of buoyancy and the ship's center of gravity. The diffraction forces are the product of body oscillations and hydrodynamic coefficients. Because of the frequency dependence of these coefficients, the Fourier transforms of the particle velocities and accelerations, $\tilde{u}$, $\tilde{v}$, $\tilde{\dot{u}}$ and $\tilde{\dot{u}}$, are used in the formulations for the diffraction part of the wave forces in long waves:

$$F'_{1,d}(t) = \int_0^\infty [m'_{11}(\omega) \cdot \tilde{\dot{u}}(\omega) + n'_{11}(\omega) \cdot \tilde{u}(\omega)] e^{i\omega t} d\omega \tag{18}$$

$$F'_{2,d}(t) = \int_0^\infty [m'_{22}(\omega) \cdot \tilde{\dot{v}}(\omega) + n'_{22}(\omega) \cdot \tilde{v}(\omega)] e^{i\omega t} d\omega \tag{19}$$

$$F'_{3,d}(t) = 0 \tag{20}$$

$$F'_{4,d}(t) = \int_0^\infty [m'_{42}(\omega) \cdot \tilde{\dot{v}}(\omega) + n'_{42}(\omega) \cdot \tilde{v}(\omega)] e^{i\omega t} d\omega + F'_{2,d}(t) \cdot \left(z_G + \frac{d_s}{2} \right) \tag{21}$$

where m'_{ij} and n'_{ij} are the cross-sectional added mass and damping coefficients respectively, z_G is the position of the center of gravity G above mean water level, d_s is the sectional draft. The cross-sectional hydrodynamic coefficients are estimated from the full body coefficients as obtained by DELFRAC and an approximation based on the added mass coefficients of a Lewis cross-section in deep water at zero-frequency [Journée & Adegeest, 2003]. The latter is only used for determination of the *distribution* of the coefficients over the ship length. The coefficients are distributed in such a way that the full body coefficients obtained by integrating the sectional values over the ship's length are equal to the DELFRAC values, which includes the influence of bottom effects and an accurate description of the hull shape.

The wave forces for pitch and yaw using strip theory follow from the calculated values for surge, sway and heave:

$$F'_5(t) = -F'_1(t) \cdot \overline{bG} - F'_3(t) \cdot x_s \tag{22}$$

$$F'_6(t) = F'_2(t) \cdot x_s \tag{23}$$

where x_s is the x-position of the cross-section relative to the center of gravity. Thus, a set of formulations has been derived to obtain the wave force without information on the wave directions which are difficult to obtain in an irregular standing wave pattern inside a harbor.

3. Prototype Measurements

3.1. *Port layout and wave measurements*

Tomakomai Port is Japan's first large excavated port and is situated at 42°38′ N latitude and 141°36′ E longitude on the southwestern part of the Hokkaido Island, 60 km south-southeast of Sapporo. Because it is an artificial port built on a flat sandy beach facing the Pacific Ocean, it had to be protected by breakwaters from drift sand to maintain its serviceability operation (see Fig. 1 for a layout).

Only sparse wave data are available, measured at three discrete locations using non-directional wave buoys. The location of the buoys is indicated in the port layout (Fig. 1). One named ST0, is placed offshore, at a depth of about 18 m and measures at a frequency of 1 Hz. The second one named ST1 is located near the berth inside the port area at 14 meters water depth; it measures at a frequency of 2 Hz. The third buoy named ST2 is placed at the entrance of the port at 18 meters water depth, just in front of the east breakwater; it measures at a frequency of 2 Hz.

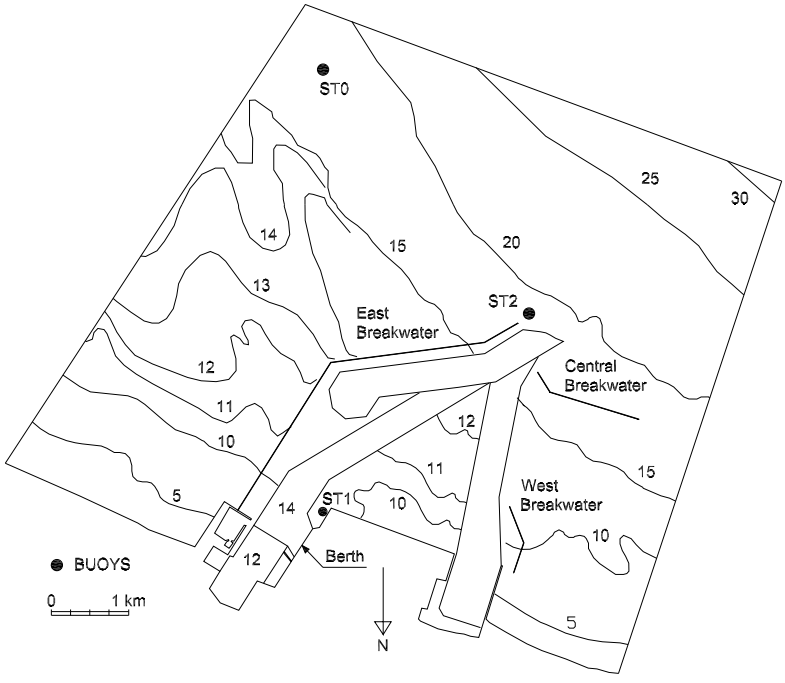

Fig. 1. Port layout, bathymetry and position of wave buoys (depths in meters).

Concerning wave directions in Tomakomai Port, 60% of the waves come from the south throughout the year [Hiraishi *et al.*, 1997; Sasa, 2002, hereafter referred to as Hi97 and Sa02] followed by those from the south-southwest, south-southeast and southwest. During 80% of the year significant wave heights do not exceed 1 meter. The frequency of occurrence of waves of 1 meter or more is higher in spring and fall. Directional spreading is not known and will be assumed according to the calibration process.

The field observations were carried out on September 18 in 1994 from 00:00 until 14:00, when the cargo vessel "E.P." was berthed at the quay with a depth of 14 m, where buoy ST1 is placed. At this day, typhoon 9424 was active southeast of Japan causing the propagation of high swell waves from offshore towards Tomakomai Port (Sa02). Significant wave heights were 3 m offshore, but lower than 0.5 m inside the port area. Despite this large reduction of the short-wave height inside the harbor, the ship was released because of large ship motions. Several lines had been broken since significant surge motions were around 4.5 m amplitude due to long-wave action (Hi97 and Sa02). After the line breaking incident, some lines were added to decrease the ship motions. In addition, initial tensions of mooring lines were lowered to prevent the breakage of ropes. Unfortunately, due to a lack of data, it is unknown when and which of the mooring lines were broken, neither the initial tensions in the mooring lines.

Table 1. Dimensions of the moored coal carrier.

Designation	Symbol	Magnitude	Unit
Length between perpendiculars	L_{PP}	215.00	m
Breadth	B	32.26	m
Depth	H	18.20	m
Actual draft	T	7.28	m
Mass displacement	Δ	40,677	tn

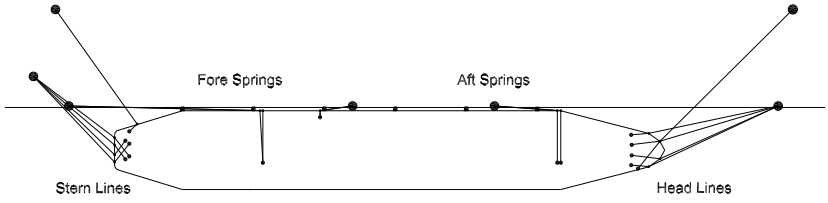

Fig. 2. Mooring arrangement of a 60,000 DWT coal carrier.

3.2. *Ship description*

The dimensions of the 60,000 DWT coal carrier "E.P." are given in Table 1. At the moment, when the ship left the berth, it was loaded with 29,446 ton, almost half loaded.

3.3. *Mooring conditions*

The data collected includes the co-ordinates of bitts, fairleads, mooring winches, number of mooring lines, force-elongation characteristics of mooring lines, co-ordinates, geometry and deflection-elongation characteristics of fenders and observed ship motions for surge and heave [Shiraishi *et al.*, 1999]. The details of the mooring lines are not exactly known. Sa02 assumed synthetic fiber ropes (pylen dabbler, diameter 65 mm) with a mean breaking strength of 657 kN at 30% elongation. Six buckling type fenders are placed against the quay wall concerned, with a height of 1.4 m and an elastic limit for the reaction force of 1153 kN at a deflection of 0.19 m. In this paper, the mooring arrangement consist of 4 bow lines, 4 stern lines, 4 breast lines and 4 spring lines (Fig. 2), according to the data provided by Shiraishi *et al.* [1999].

3.4. *Description of measurements*

Moored ship motions were observed on 1994 from September 17, 22:00 to September 18, 8:30 using a video observation technique to measure the ship movements in surge and heave. From the morning of September 18, surge motions became larger as long waves became larger. The maximum amplitude of surge was nearly 4.5 m. Predominant surge period is about 150 seconds at 8:00.

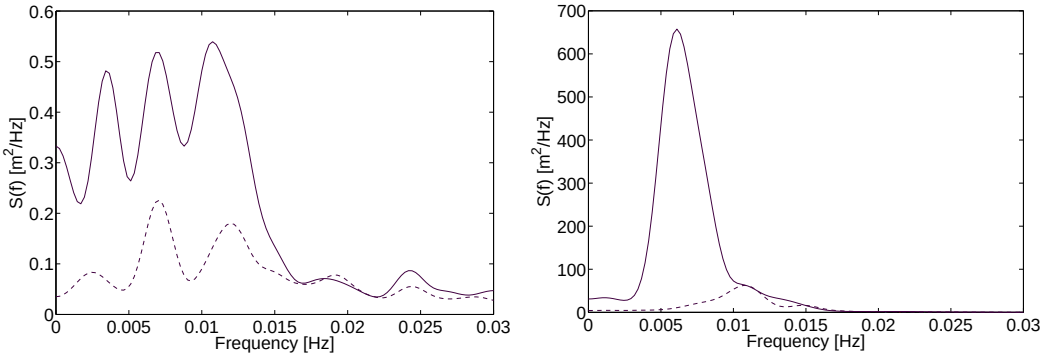

Fig. 3. Variance density of measured wave elevations at harbor buoy, ST1 (left) and measured ship's surge motion (right) from 4:00 to 5:00 (- - -), and from 7:00 to 8:00 (——) on September 18, 1994.

The data contains several gaps in some periods. For this research, two periods of one hour of ship motions are considered. These correspond to the periods from 4:00 to 5:00 and 7:00 to 8:00 on September 18. The energy spectra of the low-frequency waves measured inside the harbor and the surge motion of the ship are calculated for the two periods under analysis. In Fig. 3 waves (left) the variance density spectra show three peaks for periods 294 s (0.0034 Hz), 142 s (0.007 Hz) and 90 s (0.011 Hz), which are values that are acceptably close to the analytical values of the natural periods of the harbor basin calculated with the methods of Merian [Raichlen, 1966] and Defant [Defant, 1961], determined at approximately 300 s, 150 s and 100 s respectively, based on the average width and length of the basin.

Figure 3 waves (right) shows that the surge motion of the ship has a different period for 4:00 to 5:00 compared with 7:00 to 8:00. The surge frequency for 4:00 to 5:00 matches with the third natural frequency of the harbor, $f = 0.011$ Hz. For 7:00 to 8:00, the peak frequency of the surge motion drops to $f = 0.007$ Hz, which matches with the second natural period of the harbor. Furthermore, the enhancement of the ship motions compared with previous periods is much larger than the enhancement of the long-wave action. The loading operation was stopped at 3:30, so the ship's mass remained constant during the periods under analysis. The only plausible explanation to the change in the response is due a drastic change in the stiffness of the mooring system possibly due to line breaking, leading to a resonant response of the moored-ship system in the period from 7:00 to 8:00 as was proposed by Hi97 and Sa02.

4. Hydrodynamic Simulations

4.1. *Setup and calibration of hydrodynamic model*

The numerical model domain consists of 323×329 quadrilateral grid cells of about 25×25 m^2 each, covering the port and a part of the ocean approximately up to the 25 m depth contour, including the location of ST0. A time step of 3.6 s was selected to fulfill the Courant number requirements for stability, calculated as 1.6.

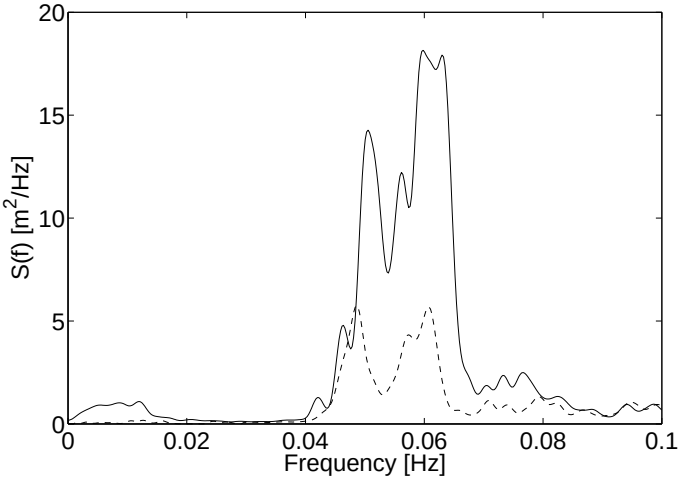

Fig. 4. Spectral density at offshore buoy (ST0) on September 18, 1994 from 4:00 to 5:00 (- - -) and from 7:00 to 8:00 (——).

The caisson breakwaters are modeled as closed boundaries, fully absorbing the short-wave energy and fully reflecting the infragravity waves.

4.2. *Input parameters of short and long waves*

As explained in Sec. 2.1, the hydrodynamic model solves the time variation of the long-wave *surface elevation* and the time variation of the short-wave *energy* on the scale of the wave groups. This distinction necessitates that a given wave spectrum (e.g. one of the measured spectra in Fig. 4 at the offshore buoy (ST0)) is separated into a short wave part and a long wave part at a split frequency, which we choose at 0.03 Hz. We then first calibrate the short-wave parameters for the short-wave energy model and then the long-wave parameters which are the boundary conditions for the long wave model.

Because the wave buoys provided no information about the directionality, the short-wave mean direction and directional spreading had to be chosen based on visual observations (personal communication with T. Hiraishi). The mean direction was selected as 180° (S) and a spreading angle of 17°. In addition, the mean direction and spreading were varied systematically to show that the offshore wave height is rather insensitive to mean direction and directional spreading within a limited range of the variation (see Table 2).

In this sensitivity analysis and the remainder of the paper, the parameter values of the wave height to depth-induced breaking parameter γ and the friction coefficient k_s were chosen as 0.35, which is a recommended value for the breaking parameter in front of reflective structures [Baquerizo & Losada, 1999; Van Gelder & Vrijling, 1999], and 0.2 m, a recommended value for the equivalent roughness in case of lack of data [WL|Delft Hydraulics, 2003], respectively. Variation of these parameters

Table 2. H_{rms} calculated for offshore station (ST0). Measured value $H_{rms} = 1.58$ m.

Spreading	Mean short-wave direction			
	158° (SSE)	180° (S)	202° (SSW)	225° (SW)
22	1.42	1.53	1.53	1.57
17	1.44	1.58	—	1.54

showed little effect on the H_{rms} results in these relatively deep waters, where wave breaking and bottom friction are of minor importance.

Besides the short wave conditions, the incident long-wave conditions also need to be determined. The bound long waves are already determined by the characteristics of the short waves. The free long waves still need to be calibrated in terms of wave height, direction and directional spreading.

Again, since wave directions were not measured, the mean direction and spreading of the incoming free long waves must be estimated. The free waves entering the model at the boundaries have been propagating in relatively shallow waters. Therefore, they have already been refracted according to the bathymetry and have been aligned around the mean direction. Subsequently, the mean wave direction is expected to be nearly perpendicular to the depth contours and shoreline and the directional spreading angle to be much smaller than the spreading of the short waves. We therefore choose the free wave mean direction as 200° (SSW), which is nearly perpendicular to the coastline (210°), with a spreading angle of 5°. The incoming free long-wave amplitude was iterated to find an optimal match between the computed and the measured low-frequency spectral shape at the offshore buoy ST0. A more detailed discussion of this iteration process and a sensitivity study on the long-wave direction and directional spreading is described in Monárdez [2004].

4.3. *Results of the low-frequency wave response*

Figure 5 shows the measured (solid line) and computed (dashed line) low-frequency response for the case of 7:00–8:00 at the offshore buoy (ST0) and harbor buoy (ST1) for the parameter settings determined above. Also shown are the results of imposing only short waves with associated bound long waves (i.e. no incoming free long waves at the boundaries see dotted line).

Figure 5 (left) shows that the results are well-simulated at the offshore buoy (ST0), which was expected due to the correction applied to the free wave components. The offshore buoy (ST0) recorded mainly free waves, because the energy content in the case of incident short and bound long waves only (dotted line) is much lower.

At the harbor buoy (ST1) the energy spectrum has a good agreement with the measured data (Fig. 5, right). At the first natural frequency of the harbor ($f = 0.0034$ Hz), the simulation differs to some extent from the measurements,

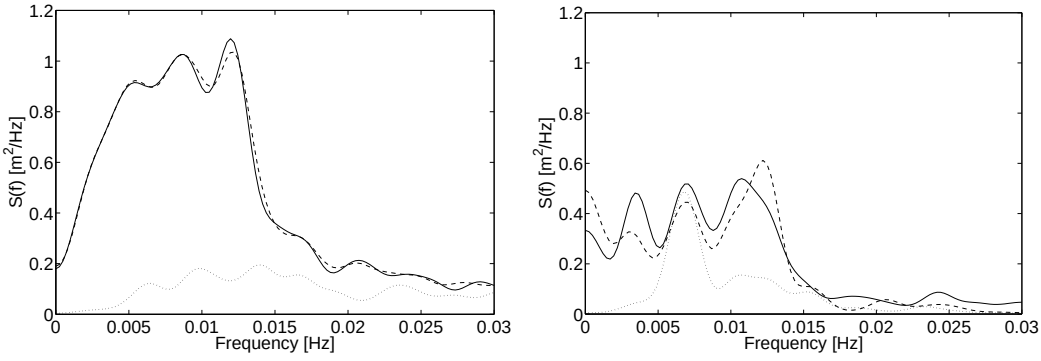

Fig. 5. Spectral energy at offshore buoy ST0 (left) and harbor buoy ST1 (right) for the case from 7:00 to 8:00. Measured data (——); simulation considering free and bound waves at the boundaries (- - -); simulation considering only bound waves at the boundaries (· · ·).

but the results are still acceptable. The energy peak at the second natural frequency of the harbor ($f = 0.007$ Hz) is well-predicted and appears only excited by released bound wave components (compare dotted and dashed lines). As stated in the Introduction, the generation mechanism of seiches by released bound waves has been described by Bowers [1977] and Wu and Liu [1990]. At the third natural frequency of the harbor ($f = 0.011$ Hz), the simulations are reasonably close to the measurements. Here the resonance is caused mostly by the free wave components. From these results, we conclude that the model is capable of reproducing the wave action inside the port area with acceptable accuracy. A possible reason why the amplification of the bound wave energy occurs at the second rather than the third natural frequency is as follows. For a given frequency the bound wave number (length) is larger (smaller) than the free wave number (length) because the bound wave number is the vectorial difference between two primary wave numbers, see e.g. Sand [1982]. Conversely, for a given wave length, the bound wave frequency is smaller than the free wave frequency. Since seiching is due to the resonance of a particular wave length in a basin, resonance will therefore occur for lower bound wave frequencies than free wave frequencies. However, in the basin, the bound waves will be released from the wave groups in which their wave lengths will lengthen over some propagation distance. This means that the precise bound wave amplification process is difficult to determine in a complex harbor, and is therefore not further explored in this paper.

The results of the long waves in the harbor for the case of 4:00–5:00 (Fig. 6 right) are less satisfactory. The first natural frequency ($f = 0.0034$ Hz) is hardly triggered in both the measurements and the simulation. The amplification at the second mode ($f = 0.007$ Hz) is underestimated while the third natural frequency ($f = 0.011$ Hz), which corresponds to the peak frequency of free waves at the ocean, is well-predicted. A possible explanation of the underestimation of the second mode is the requirement of accurate data of the short waves at the ocean. From the

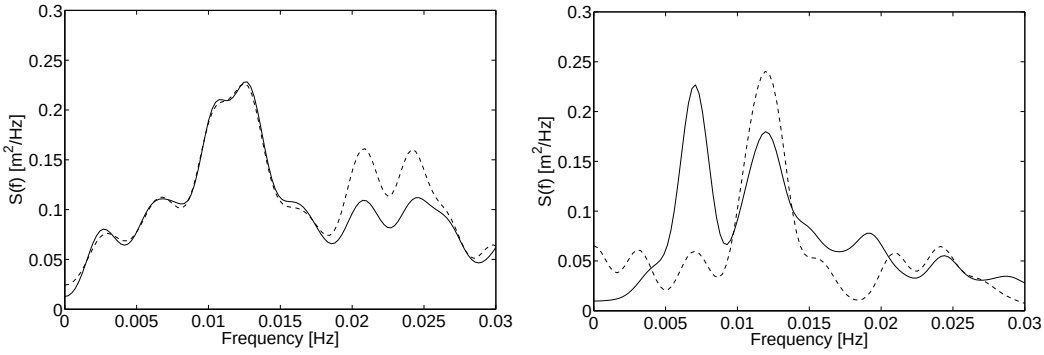

Fig. 6. Spectral energy at offshore buoy ST0 (left) and harbor buoy ST1 (right) for the case from 4:00 to 5:00. Measured data (——); simulation considering free and bound waves at the boundaries (- - -).

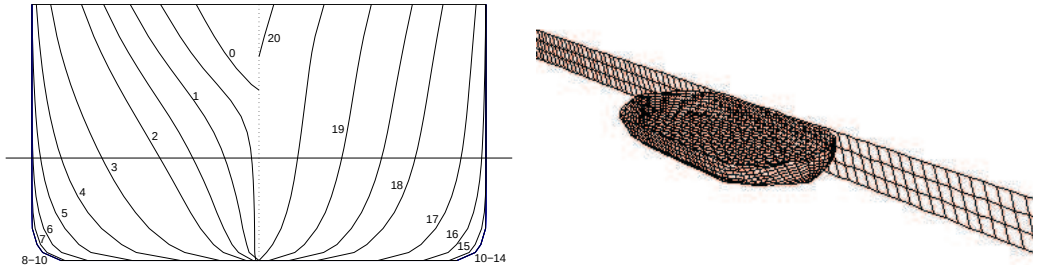

Fig. 7. Body plan of the 60,000 DWT coal carrier (left) and panel distribution on the ship and the quay wall (right).

investigation of the case of 7:00–8:00, it was concluded that a detailed input of the short-wave spectrum at sea is important for correct modeling of the response in the mid-infragravity frequency range. Hence, small measurement errors or incorrect input of short waves at the boundaries can lead to these significant differences. The latter explanation may play a role here, because the model parameters, such as the mean wave direction and the directional spreading, are calibrated for the case of 7:00–8:00 and were then used again for the case of 4:00–5:00. In the next section, it will be shown that the third peak is the most important for ship response, so the poor modeling of the second peak will have no effect on those results.

5. Simulation of Ship Motions

5.1. *Hydrodynamic coefficients*

The hydrodynamic coefficients required for the determination of the wave forces and for the calculation of ship motions, are calculated by the panel model DELFRAC. The submerged hull is divided into 1,184 flat quadrilateral panels, the quay wall is modeled as a long array of panels and the water depth is assumed constant ($h = 14$ m) for this computation (see Fig. 7).

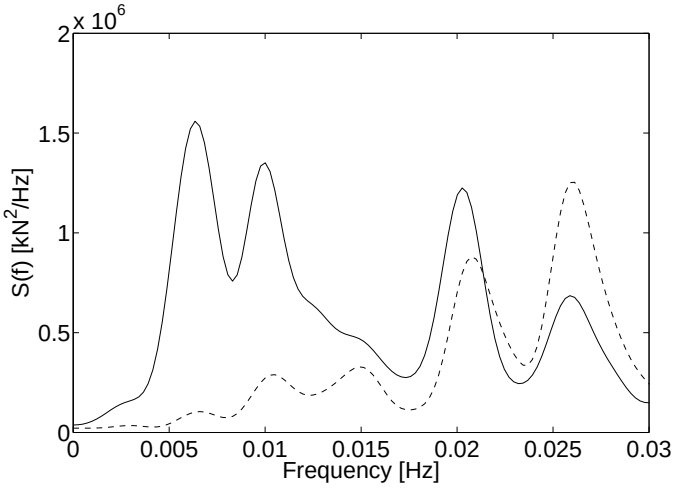

Fig. 8. Spectral density of calculated low-frequency wave forces. Periods from 4:00 to 5:00 (- - -) and 7:00 to 8:00 (——).

5.2. *Wave exciting forces*

For the determination of the wave forces on the floating object, the approach of Ordinary Strip Theory is used. For the case of irregular waves, the Fourier Transform of the particles velocities and the accelerations is applied, because the hydrodynamic coefficients are not constant over the wave frequencies. After the spectral components have been obtained, the wave loads are calculated as a function of time for the six degrees of freedom. The long-wave forces are calculated with the *lf-strip* numerical model at the positions of 25 cross-sections (Fig. 8). The sectional forces are integrated over the ship length to obtain the total wave force. The spectra of wave forces for the two cases are plotted in Fig. 8. It is noted that the low-frequency wave force spectra have four energy peaks. The lowest two frequency peaks of the force spectrum correspond to the highest two excited natural frequencies of the harbor basin ($f = 0.007$ Hz and $f = 0.011$ Hz). There are two more frequency peaks at higher frequencies in the force spectrum — Fig. 8 ($f = 0.021$ Hz and $f = 0.026$ Hz), which do not have an analogous energy peak in the low-frequency wave energy spectrum (Fig. 3). The reason for these peaks in the force spectrum is due to the wavelength of the corresponding long waves ($L = 450$ to 580 m), which is about twice the length of the ship. Then the gradient in the water surface leads to considerable surge forces. The lowest energy peak of the long-wave energy spectra ($f = 0.0034$ Hz, see Fig. 3) does not have a corresponding peak in the spectral density of the long-wave forces. Because the wavelength at this frequency is very large ($L = 1000$ m), which is much larger than the ship length, it leads only to heave forces and hardly any surge forces.

5.3. *Ship's dynamic simulations*

The only free parameters to calibrate in the ship's dynamic model are the fender friction and the initial tension in the mooring lines. The viscous damping coefficient for surge is approximated as 200 tn/m, based on experimental investigation of a tanker in current [OCIMF, 1997]. The fender friction coefficient is calibrated at 0.5, although the sensitivity to fender friction appeared to be low for the low pretension in mooring lines in this case.

The initial tension is calibrated considering the information from the site and previous studies. According to Sa02, some mooring lines had been broken during the loading operation, shortly before 7:00. After the line break accident, some lines were added to decrease the ship motions. In addition, initial tensions of mooring lines were lowered to prevent the breakage of ropes. Unfortunately, it is unknown when and which of the mooring lines were broken, neither has initial tensions in the mooring lines. To overcome this lack of information, Sa02 assumed two cases: the first case with an initial tension of 4 ton in each mooring line with a winch; the second case without any initial tension. The calculated significant surge motions were 5.91 m and 7.66 m and the significant surge period 95 s and 149 s for the first and second case, respectively. Therefore, in Sa02, the frequency of the motion was better approached for the case without initial tension, while the amplitude of the surge motion was better approached for the case with initial tension. Sasa's computations are based on a linear model for long-period harbor oscillations forced by free long waves, accurate calculation of the Froude-Krylov force and an approximation for the diffraction forces on the ship.

In the present study, to investigate the sensitivity of the surge motion on the pretension value, a large number of simulations for different pretensions have been carried out. A few of the results are given in Fig. 9 for different values of the pretension in bow and stern lines. For both cases, 3 ton pretension was assumed

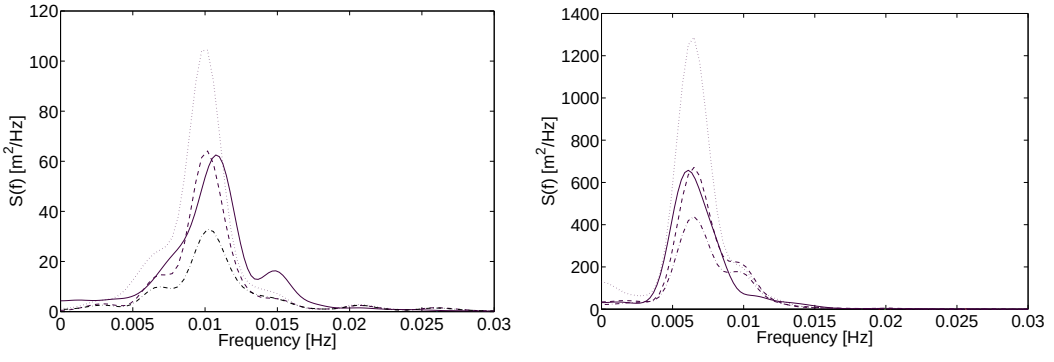

Fig. 9. Surge motion spectra for the bulk carrier for different values of pretension in bow and stern lines. Case from 4:00 to 5:00 (left), measured data (——), simulations with 2 ton pretension (· · ·), 3 ton (- - -) and 4 ton (· - · - ·). Case from 7:00 to 8:00 (right), measured data (——), simulations with 2.5 ton pretension (· · ·), 3.5 ton (- - -), 4.5 ton (· - · - ·).

Table 3. Comparison of infragravity waves in the harbor and surge motions of the ship.

Period	Offshore (ST0) Measured			Harbor (ST1) Measured		Harbor (ST1) Simulated		Surge motion Measured		Surge motion Simulated	
	H_s [m]	$H_{s,l}$ [m]	$T_{s,l}$ [s]	$H_{s,l}$ [m]	$T_{s,l}$ [s]	$H_{s,l}$ [m]	T_{sl} [s]	$X_{1,s}$ [m]	T_s [s]	$X_{1,s}$ [m]	T_s [s]
4–5 am	1.26	0.23	64	0.19	78	0.17	73	2.35	91	2.07	95
7–8 am	2.43	0.48	97	0.32	105	0.31	109	6.54	143	6.60	138

in the spring lines. For 7:00–8:00, one spring line was assumed to be broken as was suggested by Sa02.

The peak period of the ship motions has shifted between 5:00 and 7:00. Before the line break accidents the pretension in spring lines caused a larger stiffness of the moored ship system than after the line breaking. Hence, for 4:00–5:00 the ship motions are amplified at the third natural frequency of the harbor ($f = 0.011$ Hz) and for 7:00–8:00 the amplification is at the second mode of the harbor basin ($f = 0.007$ Hz). Because the third mode of the harbor was simulated well for 4:00–5:00 and this is close to the natural surge frequency of the ship, the surge motions are simulated correctly as well.

Statistical values are calculated from the measured wave elevation and ship motions and compared with the simulations. Values are summarized in Table 3. For 4:00–5:00 the simulation with 3 ton pretension in all lines is adopted and for 7:00–8:00, 3.5 ton in head and stern lines.

The results of the simulations show that, given the information of long and short waves at the ocean, it is possible to accurately predict the wave and ship motions in the harbor, although the vessel motions are very sensitive to the pretension in mooring lines.

6. Mitigation Measures

The measures to counter the effect of the long-wave action in the port can be divided in two types. One type is based on changing the hydrodynamic behavior of the harbor, affecting the infragravity wave field pattern itself. These solutions consider extensive measures, such as basin modifications, breakwater extensions or construction of resonators. These measures are expensive by nature and a study on cost-effectiveness study must be carried out. The effectiveness of the different alternatives can be evaluated in further studies. A second type of solution is to allow the seiche action inside the port, by reducing the ship motions using an effective mooring system operation. During the analyzed periods, the ship's motions were amplified due to resonance of the moored ship system and the excitation. By changing the natural frequency of the moored ship system, it could be possible to reduce the ship

motions. This solution is proposed, because it is easily implemented and does not have any extra cost involved.

6.1. *Effect of pretension*

Consider the case in study from 7:00 to 8:00. As it was mentioned above, the aft and fore spring were broken or the pretension could have been reduced, in order to prevent rope breaking. With this breaking or the reduction of pretension, the natural frequency of the moored ship system was shifted only slightly, since the pretension at the lines was relatively small. If the pretension on the mooring line would have been increased, the effect would have been different, since the stiffness of the mooring line is increased when the pretension is increased. Then the natural frequency of the moored ship system is increased as well, away from the range of the natural frequency of the harbor, and the ship's movements would be reduced. In order to evaluate this counter measure, different pretensions are evaluated. The ship motions are calculated in the period from 7:00 to 8:00. The results are presented in Table 4.

As can be seen from Table 4, the influence of increasing the pretension is clear, the surge motion is reduced significantly, and the sway motion is almost stopped. The maximum heave motion, which is not given in the table, is nearly independent of the pretension and only 0.4 m in these low, long waves. The surge movement is reduced from almost 10 m to 1 m in the case of 20 ton pretension, which is a workable condition for on- and off-loading of bulk carriers. Nonetheless, it should be stressed that wave induced ship motions are not the only cause for downtime of the unloading process. In the case described in this paper, the unloading was also stopped due to heavy wind loads on the quay equipment. In such a case, safe mooring should be maintained without the risk of line breaking accidents.

The spectral energy of the surge and sway motions calculated from Table 4 is plotted in Fig. 10. The peak frequency of the surge motion shifts for larger pretension values from 0.006 to 0.011 Hz, which matches with the third natural frequency of the harbor. The surge energy content is reduced significantly due to two effects: the shift in the natural frequency of the system and the influence of the friction of the fender force, which can be considerable for large values of the pretension. The sway motion also has distinct behavior for larger pretension values. The low-frequency

Table 4. Double amplitudes of maximum surge and sway displacements [m] for different pretensions in mooring lines.

Designation	0 tn	5 tn	10 tn	15 tn	20 tn
surge	9.9	7.0	4.0	1.5	1.1
sway	1.2	0.3	0.1	0.2	0.2

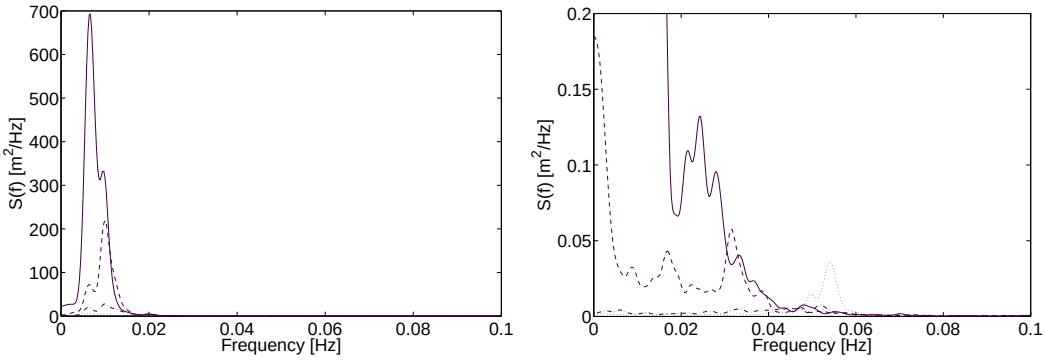

Fig. 10. Surge (left) and sway (right) motion spectra for different pretensions. Simulation without initial tension in springs and 2.5 ton in bow and stern lines (——); 5 ton (- - -), 10 ton (· - · - ·) and 20 ton (· · ·) pretension in all lines.

Table 5. Maximum forces [kN] in mooring lines for different pretensions (7:00 to 8:00).

Designation	0 tn	5 tn	10 tn	20 tn	30 tn
Bow line	230	177	220	288	144
Aft spring	219	147	146	180	228

motion is almost stopped and a small high-frequency peak emerges. The system is then much stiffer, mainly because the ship is pushes against the stiff fenders.

The forces in the mooring lines were analyzed, in order to check if the increase in the pretension can break the ropes. Applying a pretension of 20 ton leads to a maximum tension of 288 kN in the ropes (Table 5), which is still far below the design load of 657 kN. It can be concluded that an increase of the pretension leads to a considerable decrease of the ship motions under a small increase of the maximum line loads. Applying pretension can even reduce the maximum line loads, if the natural surge period is shifted away from one of the resonant periods of the harbor.

7. Conclusions and Recommendations

A method has been developed to simulate the moored ship motions due to long-wave action inside a harbor basin. The method is based on a coupling of three numerical models: (1) a depth-averaged non-linear flow model with short-wave forcing for the calculation of infragravity wave penetration in the harbor, (2) a strip theory based method to obtain the low-frequency wave forces from the computed wave slopes and fluid motions and (3) a ship motion simulation model which takes into account the non-linear properties of mooring lines and fenders. The calculations of infragravity waves in the harbor agree reasonably with the measurements. The model predicts the right natural frequencies of the harbor basin and the corresponding amplification factors for both the lowest resonant frequencies and the higher ones. Nonetheless,

there is some uncertainty due to the lack of information on the wave directions, which had to be estimated. For a more accurate validation of the calculation process, wave directions should be recorded.

The simulation results show that both free long waves and bound waves, associated with wave groups at the ocean, can excite harbor oscillations. This implies that detailed information of both long and short waves at the ocean is required for accurate modeling of wave penetration in the harbor.

The simulations of ship motions using the calculated infragravity waves at the location of the ship show good correspondence with the measured surge movements. Only one of the resonant peaks of the harbor basin remains in the spectrum of the surge motions, which is closest to the natural frequency of the moored ship. The pretension appears to be a very important parameter. Increasing the value of the pretension initially leads to smaller movements, but increases the line loads. Besides, the natural frequency of the moored ship is also increased. Hence, by either tensioning or slackening of mooring lines the natural frequency of the mooring system shifts away from the harbor oscillation frequency. This can be a useful and easy solution to decrease the movements of a moored ship during operation in a port subjected to low-frequency oscillations.

Acknowledgments

This project has been sponsored by the Lamminga Fund (Delft University of Technology, Faculty of Civil Engineering) and the Netherlands Center for Coastal Research (NCK). The authors are very thankful to Dr. Hiraishi from PARI, Japan, for making available the measured data from Tomakomai.

References

Baquerizo, A. & Losada, M. A. [1999] "Wave height to depth ratio in front of coastal structures," in *Proc. Int. Conf. on Coastal Structures* (Santander, Spain), Vol. 1, pp. 23–28.

Biésel, F. [1952] "Équations générales au second ordre de la houle irrégulière," *La Houille Blanche* **7**, 371–376.

Bingham, H. B. [2000] "A hybrid Boussinesq-panel method for predicting the motion of a moored ship," *Coastal Engineering* **40**(1), 21–38.

Booij, N., Ris, R. C. & Holthuijsen, L. H. [1999] "A third-generation wave model for coastal regions. Part I, model description and validation," *J. Geophys. Res.* **104**(C4), 7649–7666.

Bowers, E. C. [1977] "Harbour resonance due to set-down beneath wave groups," *J. Fluid Mech.* **79**(1), 71–92.

Defant, A. [1961] *Physical Oceanography*, Vol. II (Pargamon, New York, USA).

Dingemans, M. J. F., Petit, H. A. H., Meijer, T. J. G. P. & Kostense, J. K. [1991] "Numerical evaluation of the third-order evolution equations for weakly nonlinear water waves propagating over uneven bottoms," in *Computer Modelling in Ocean Engineering 91* (Barcelona, Spain), pp. 361–370.

Haskind, M. [1957] "The exciting forces and wetting of ships in waves (in Russian)," *Izvestia Akademii Nauk SSSR, Otdelenie Tskhnicheshikh Nauk* **7**, 65–79.

Hiraishi, T., Atsumi, Y., Kunita, A., Sekiguchi, S. & Kawaguchi, T. [1997] "Observations of long period wave and ship motion in tomakomai-port," in *Proc. 7th ISOPE Conf.* (Honolulu, USA), Vol. III, pp. 546–551.

Journée, J. M. J. & Adegeest, L. J. M. [2003] "Theoretical manual of strip theory program 'SEAWAY for Windows' " (Report No. 1370), Delft, The Netherlands: Delft University of Technology.

Longuet-Higgins, M. S. & Stewart, R. W. [1962] "Radiation stress and mass transport in gravity waves, with aplication to 'surf beats'," *J. Fluid Mech.* **13**, 481–504.

Longuet-Higgins, M. S. & Stewart, R. W. [1964] "Radiation stresses in water waves; a physical discussion with applications," *Deap-Sea Res.* **11**, 529–562.

Monárdez, P. [2004] *Numerical Modelling of Long Waves in Harbours.* MSc thesis, Unesco-IHE Institute for Water Education, Delft, The Netherlands.

Munk, W. H. [1949] "Surf beats," *Eos Trans. AGU* **30**(6), 849–854.

Mynett, A. E., Keuning, P. J. & Vis, F. C. [1985] "The dynamic behaviour of moored vessels inside a harbour configuration," in *Int. Conf. on Numerical and Hydraulic Modelling of Ports and Harbours* (Birmingham, UK), pp. 211–220.

OCIMF [1997] *Mooring Equipment Guidelines*, (2nd edition) (Oil Companies International Marine Forum, Witherby, London, UK).

Ohyama, T. & Tsuchida, M. [1997] "Expanded mild-slope equations for the analysis of wave-induced ship motion in a harbor," *Coastal Engineering* **30**, 77–103.

Pinkster, J. A. [1995] "Hydrodynamic interaction effects in waves," in *Proc. 5th ISOPE Conf.* (The Hague, The Netherlands), Vol. III, pp. 414–419.

Raichlen, F. [1966] "Harbor resonance," in *Estuary and Coastline Hydrodynamics*, ed. Ippen, A. T. (McGraw-Hill, New York, USA), pp. 281–340.

Reniers, A. J. H. M., Roelvink, J. A. & Van Dongeren, A. R. [2000] "Morphodynamic response to wave group forcing," in *Proc. 27th ICCE* (Sydney, Australia), pp. 3218–3228.

Reniers, A. J. H. M., Roelvink, J. A. & Thornton, E. B. [2004] "Morphodynamic modeling of an embayed beach under wave group forcing," *J. Geophys. Res.* **109**, C01030.

Rodi, W. [1980] "Turbulence models and their application in hydraulics," Delft, The Netherlands: Int. Ass. for Hydraulic Res.

Sand, S. E. [1982] "Long waves in directional seas," *Coastal Engineering* **6**, 195–208.

Sasa, K. [2002] *A Study on Prediction of Ship Operation Using Numerical Simulations and Observed Oceanographic Database Under Swells and Long Period Waves in Harbour Facing to Open Seas*, PhD thesis, Kobe University of Mercantile Marine, Kobe, Japan.

Shiraishi, S., Kubo, M., Sakakibara, S. & Sasa, K. [1999] "A study on numerical simulation methods to reproduce long-period ship motions," in *Proc. 9th ISOPE Conf.* (Brest, France), Vol. 3, pp. 536–543.

Tucker, M. J. [1950] "Surfbeats: sea waves of 1 to 5 minutes' perod," *Proc. R. Soc Lond. A* **202**, 565–573.

Van der Molen, W., Weiler, O. M. & Ligteringen, H. [2003] "Long-period wave forces on a moored ship in a harbour using a strip theory approach," in *Proc. 2nd Int. Conf. on Port and Maritime R&D and Technology* (Singapore), Vol. 1, pp. 113–120.

Van Dongeren, A. R., Reniers, A. J. H. M., Battjes, J. A. & Svendsen, I. A. [2003] "Numerical modeling of infragravity waves response during DELILAH," *J. Geophys. Res.* **108**(C9), 3288.

Van Gelder, P. H. A. J. M. & Vrijling, J. K. [1999] "On the distribution function of the maximum wave height in front of reflecting structures," in *Proc. Int. Conf. on Coastal Structures* (Santander, Spain), Vol. 1, pp. 37–46.

Van Giffen, I. K., Battjes, J. A., Van Dongeren, A. R. & Moes, J. [2003] "Simulation of long waves in Saldanha Bay," in *Long Wave Symposium* (Tessaloniki, Greece), pp. 113–122.

WL|Delft Hydraulics [2003] "Delft3D-Flow simulation of multi-dimensional hydrodynamic flows and transport phenomena, including sediments," (User manual), Delft, The Netherlands: WL|Delft Hydraulics.

Wu, J. K. & Liu, P. L. F. [1990] "Harbour exitations by incident wave groups," *J. Fluid Mech.*, **217**, 595–613.